Study of Strain and Temperature Dependence of Metal Epitaxy

C. Ratsch, P. Ruggerone, and M. Scheffler

Fritz-Haber-Institut der Max-Planck-Gesellschaft, Faradayweg 4-6,
D-14195 Berlin-Dahlem, Germany

August 21, 2010

1   INTRODUCTION

Metallic films are important in catalysis, magneto-optic storage media, and interconnects in microelectronics, and it is crucial to predict and control their morphologies. The evolution of a growing crystal is determined by the behavior of each individual atom, but technologically relevant structures have to be described on a time scale of the order of (at least) tenths of a second and on a length scale of nanometers. An adequate theory of growth should describe the atomistic level on very short time scales (femtoseconds), the formation of small islands (microseconds), as well as the evolution of mesoscopic and macroscopic structures (tenths of seconds). Different theoretical approaches to the description of growth phenomena address different time

Table 1:   The time and length scales handled by different theoretical approaches to study growth.

	Type of information	Time scale	Length scale
Density functional theory calculations	Microscopic	-	$\leq 10^3$ atoms
Ab initio molecular dynamics	Microscopic	$t \leq 10$ ps	$\leq 10^2$ atoms
Semi-empirical molecular dynamics	Microscopic	$t \leq 1$ ns	$\leq 10^3$ atoms
Kinetic Monte Carlo	Microscopic to Mesoscopic	1 ps $\leq t \leq$ 1 hour	≤ 1 μm
Rate equations	Averaged	0.1 s $\leq t \leq \infty$	All
Continuum equations	Macroscopic	1 s $\leq$ t $\leq \infty$	≥ 10 nm

1

and length scales, and an overview is given in Table 1. These different techniques should be regarded as complementary to each other rather than as alternatives, and we will show in this article how some of them may successfully be combined.

The development of efficient algorithms combined with the availability of cheaper and faster computers has turned density functional theory (DFT) into a reliable and feasible tool to study the microscopic aspects of growth phenomena (and many other complex processes in materials science, condensed matter physics, and chemistry). These calculations provide the so-called potential energy surface (PES, also often called total energy or Born-Oppenheimer surface) that is the potential energy experienced by a particle during chemical reactions and diffusion. The basic concepts behind DFT are sketched in Section 2. A single microscopic process on such a PES can be characterized by either doing a molecular dynamics (MD) simulation or by using transition state theory. Both approaches typically will give the same result. Problems may occur when the energy barrier is comparable to the thermal energy and correlated effects cannot be neglected. An overview over the different processes and how they can be described within transition state theory is given in Section 3.

Technologically relevant applications of growth often involve disparate materials with different lattice constants. However, it is not understood so far how strain in a system influences the most fundamental process that occurs during epitaxial growth, the diffusion of a single adatom on a substrate. It is the aim of this article to discuss the current understanding of this aspect. In Section 4 some recent results for the strain dependence of surface diffusion that is determined by an energy barrier and a prefactor will be presented. While the DFT results were obtained for only a few metallic systems, we assert that the physical trends discussed are rather general.

A DFT total energy calculation by its nature is primarily a *static* calculation. An accurate way to describe the *dynamical* evolution of a growing crystal is given by MD simulations. It is not possible to carry out such a simulation on mesoscopic and/or macroscopic time and length scales. Ab initio MD runs usually can cover at most times of picoseconds, whereas semi-empirical MD runs may extend up to some nanoseconds (at the cost of the accuracy). This is because an MD time step cannot be longer than the inverse of a typical phonon frequency. For example, a MD run simulates the entire sequence of unsuccessful attempts occurring between two successful diffusion events that may be separated by interval of the order of nanoseconds. Thus, MD can model only very few events, and a proper statistics cannot easily be obtained for growth processes. Moreover, since growth patterns usually develop on a time scale of seconds, the inadequacy of MD is evident. Finally, the growth structures involve large numbers of particles ($\sim 10^2$ to 10^4), far beyond the reach of MD (simulations with $\sim 10^2$ atoms are hardly feasible, and only for very short times). Because an adequate treatment of the statistical nature of the problem is typically not achieved, we believe that the value of MD is often overstated, and the method of choice for studying the spatial and temporal development of growth is kinetic Monte Carlo (KMC).

The growing crystal defines a lattice system onto which the non-crystalline growth units (atoms or molecules) are deposited. In the case of growth from solution or from vapor one may assume with sufficient generality that the growth units impinge on the surface (or, more exactly, on the solid-vapor) interface at random with an average frequency. The same random character belongs to the diffusion of growth units on the surface. It is therefore natural to describe deposition, desorption, and diffusion mechanisms as stochastic processes, and this matches very well with the stochastic nature of the Monte Carlo method. A brief introduction to this method and its combination with microscopic parameters obtained from *ab initio* parameters is given in Section 5. It is shown that realistic *ab initio* kinetic Monte Carlo simulations are able to predict an evolving mesoscopic structure on the basis of microscopic details.

In order to compare quantitatively results from a Monte Carlo simulations with experimentally measured quantities, such as for example the density of islands on the surface, one needs to take a statistical average over this quantity. In a KMC simulation this is obtained by doing a simulation on a sufficiently large lattice. An alternative and more elegant approach is the construction of mean field equations that by definition only contain averaged quantities. An example are rate equations discussed briefly in Section 2. Numerical solution of these equations can give the density of islands, but without microscopic details. This ansatz currently is not sufficiently advanced to make reliable predictions for experimentally relevant quantities and needs to be developed further. As the final goal a proper mean field approach should yield the same results as the statistical average over the results of a more detailed microscopic approach. The inclusion of more details (that in principle is possible) unfortunately makes a mean field or continuum approach less tractable, so that new techniques have to be developed.

2   BASIC CONCEPTS OF DENSITY FUNCTIONAL THEORY

The total energy of an N-electron, poly-atomic system is given by the expectation value of the many-particle Hamiltonian using the many-body wave-function of the electronic ground state. For a solid or a surface the calculation of such an expectation value is impossible within the framework of a wave-function approach. However, Hohenberg and Kohn [1] have shown that the ground-state total energy can also be obtained without explicit knowledge of the many-electron wave-function by minimizing an energy functional $E[n]$. This is the essence of density-functional theory (DFT), which is primarily (though in principle not exclusively) a theory of the electronic ground state, couched in terms of the electron density $n(\mathbf{r})$ instead of the many-electron wave-function $\Psi(\{\mathbf{r}_i\})$.

The important theorem of Hohenberg and Kohn [1] (see also Levy [2]) states: The specification of a ground state density $n(\mathbf{r})$ determines the corresponding external

potential $v^{\text{ext}}(\mathbf{r})$ *uniquely* (to within an additive constant),

$$n(\mathbf{r}) \rightarrow v^{\text{ext}}(\mathbf{r}) \quad . \tag{1}$$

The external potential $v^{\text{ext}}(\mathbf{r})$ is typically (and definitely for our purpose here) the Coulomb potential due to the nuclei, assumed at fixed positions as they are much heavier than the electrons (Born-Oppenheimer approximation). While the other direction $[v^{\text{ext}}(\mathbf{r}) \rightarrow n(\mathbf{r})]$ is well known to exist (because $v^{\text{ext}}(\mathbf{r})$ determines the many-particle Hamiltonian H) Eq. (1) is less obvious. The theorem enables to transform the variational problem of the many-particle Schrödinger equation into a variational problem of an energy functional:

$$E_0 \leq \langle \Psi | H | \Psi \rangle = E_v[\Psi[n]] = E_v[n] \quad , \tag{2}$$

with E_0 the energy of the ground state, and $E_v[n] = \int d\mathbf{r}\, v^{\text{ext}}(\mathbf{r})n(\mathbf{r}) + G[n]$. The variable is $n(\mathbf{r})$ (the electron density of any N-electron system), and $v^{\text{ext}}(\mathbf{r})$ is kept fixed. $G[n]$ is a *universal* functional independent of the system, i.e., independent of $v^{\text{ext}}(\mathbf{r})$. The main advantage of this approach is that $n(\mathbf{r})$ only depends on three variables, while $\Psi(\{\mathbf{r}_i\})$ depends on all the coordinates of the N electrons [3]. Thus, it is plausible that the variational problem of $E_v[n]$ is easier to solve than that of $\langle \Psi | H | \Psi \rangle$, yet the result for the ground-state energy and the ground state electron density will be the same. The total energy is [4]

$$E^{\text{tot}}(\{\mathbf{R}_J\}) = E_0(\{\mathbf{R}_J\}) + \frac{1}{2} \sum_{J,J',J \neq J'} \frac{Z_J Z_{J'}}{|\mathbf{R}_J - \mathbf{R}_{J'}|} \quad , \tag{3}$$

where $\{\mathbf{R}_J\}$ includes all atoms, and Z_J is the nuclear charge.

An important problem remains, namely that the exact form of the functional $G[n]$ is unknown. Earlier work (in particular the Thomas-Fermi approach) had shown that the treatment of the kinetic energy $\langle \Psi | -\frac{1}{2}\nabla^2 | \Psi \rangle$ is of particular importance and Kohn and Sham [5] therefore wrote the energy functional in the form

$$E_v[n] = T_s[n] + \int d\mathbf{r}\, v^{\text{ext}}(\mathbf{r})n(\mathbf{r}) + \frac{1}{2} \int d\mathbf{r}\, v^{\text{H}}(\mathbf{r})n(\mathbf{r}) + E^{\text{xc}}[n] \quad , \tag{4}$$

where $T_s[n]$ is the functional of the kinetic energy of a system of non-interacting electrons with density $n(\mathbf{r})$, and $v^{\text{H}}(\mathbf{r}) = \int d\mathbf{r}' \frac{n(\mathbf{r}')}{|\mathbf{r}-\mathbf{r}'|}$ is the Hartree potential that describes the electrostatic interaction between electrons. $E^{\text{xc}}[n]$, the so-called exchange-correlation functional, accounts for the Pauli principle, dynamical correlations due to the Coulomb repulsion, and the correction of the self-interaction included for convenience in the Hartree term. With Eq. (4) the problem of the unknown functional $G[n]$ is mapped onto one that involves $T_s[n]$ and $E^{\text{xc}}[n]$. Although the functional $T_s[n]$ is not known explicitly in a mathematically closed form, it can be evaluated exactly by

using the following "detour" proposed by Kohn and Sham. The variational principle applied to Eq. (4) leads to

$$\frac{\delta E_v[n]}{\delta n(\mathbf{r})} = \frac{\delta T_s[n]}{\delta n(\mathbf{r})} + v^{\text{eff}}(\mathbf{r}) = \mu \quad , \tag{5}$$

where μ is the Lagrange multiplier associated with the requirement of a constant particle number and thus equals the electron chemical potential. The effective potential is defined as

$$v^{\text{eff}}(\mathbf{r}) = v^{\text{ext}}(\mathbf{r}) + v^{\text{H}}(\mathbf{r}) + v^{\text{xc}}(\mathbf{r}) \quad , \tag{6}$$

with $v^{\text{xc}}(\mathbf{r}) = \delta E^{\text{xc}}[n]/\delta n(\mathbf{r})$, and $n(\mathbf{r})$ is a ground-state density of any non-interacting electron system, i.e.,

$$n(\mathbf{r}) = 2\sum_{i=1} f_i |\phi_i(\mathbf{r})|^2 \quad , \tag{7}$$

where we introduced the occupation numbers f_i. The factor 2 accounts for the spin degeneracy. Since $T_s[n]$ is the kinetic energy functional of non-interacting electrons, Eq. (5) [together with Eq. (7)] is solved by

$$\left[-\frac{1}{2}\nabla^2 + v^{\text{eff}}(\mathbf{r}) \right] \phi_i(\mathbf{r}) = \epsilon_i \phi_i(\mathbf{r}) \quad . \tag{8}$$

These are the Kohn-Sham equations, that are to be solved self-consistently together with Eqs. (6) and (7). In principle, this gives the exact ground-state electron density and total energy of a system of interacting electrons. However, the functional $E^{\text{xc}}[n]$ is still unknown. Some general properties of this functional and values for some special cases are known. Detailed and very accurate understanding exists for systems of constant electron density. These results for $\epsilon^{\text{xc}} := \epsilon^{\text{xc}}_{\text{LDA}}(n)$ are then used in the functional

$$E^{\text{xc}}_{\text{LDA}}[n] = \int d\mathbf{r}\, n(\mathbf{r})\epsilon^{\text{xc}}_{\text{LDA}}(n(\mathbf{r})) \quad , \tag{9}$$

which is the local-density approximation (LDA) [5]. Thus, in the LDA the many-body effects are included such that for a homogeneous electron gas the treatment is exact and for an inhomogeneous system exchange and correlation are treated by assuming that the system can be composed from many small systems with a locally constant density.

The LDA can be improved by including the dependence on the density gradient which leads to the generalized gradient approximation (GGA). Several different GGA's were proposed in the literature [6, 7, 8, 9, 10] and have been used successfully for DFT calculations for atoms, molecules, bulk solids, liquids, and surfaces (an overview can be found in Refs. [11, 12]), but also limitations have been pointed out [13, 14]. It is by now clear that the lattice constants calculated with a GGA are typically larger than those obtained with the LDA, with the experimental values usually being in between. Binding energies (or cohesive energies) of molecules and solids are clearly improved by the GGA as well as energy barriers of chemical reactions. (see

Ref. [15] and references therein). A general rule of thumb for the use of LDA or GGA is still missing and tests should be carried out for each specific problems. The total energies are changed when going from the LDA to the GGA, thus for surface diffusion the changes in energy barriers, i.e., in total energy *differences*, may be pronounced as well although the rank of the processes is not altered (see Refs. [16, 17]). The GGA data are usually more reliable, but still careful calculations with various forms of GGA must be performed.

The general method described above can be transformed into an operative tool following diverse schemes that essentially differ in the basis employed to expand the electronic wave function. A widely used basis set (also chosen for the calculations presented below) consists of plane waves (see Refs. [18, 19]) but other choices are possible [20, 21]. A deeper discussion of the implementations of the DFT plane-wave basis set method for the study of growth phenomena can be found in Ref. [22].

3   ATOMISTIC PROCESSES

The different atomistic processes encountered by adatoms that are deposited onto a surface are illustrated in Fig. 1. After deposition (a) atoms can diffuse across the surface (b) and will eventually meet another adatom to form a nucleus (c) or get captured by an already existing island or a step edge (d). Once an adatom has been captured by an island, it may either break away from the island (*reversible aggregation*) (e) or remain bonded to the island (*irreversible aggregation*). An atom that is bonded to an island may diffuse along its edge (f) until it finds a favorable site. As long as the coverage of adsorbed material is low (say $\Theta \leq 10$ %), deposition on top of islands is insignificant and nucleation of islands on top of existing islands practically does not occur. However, if the step down motion (g) is hindered by an additional energy barrier, nucleation of island on top of islands (h) becomes likely at some critical coverage. In this article we will mainly focus on the migration of adatoms on the flat terrace or along step edges and will not discuss effects that are due to mass transport between different layers. Moreover, we will say nothing about the possibility of long jumps even though it most likely plays a role for certain systems as it has been observed with the field ion microscope for Pd on W (211) by Senft and Ehrlich [23], and very recently in a scanning tunneling microscopy study for Pt on Pt (011) by Linderoth *et al.* [24].

3.1   Transition State Theory

To understand the diffusion of an adatom on a surface we need to calculate its potential-energy surface (PES):

$$E^{\mathrm{PES}}(X_{\mathrm{ad}}, Y_{\mathrm{ad}}) = \min_{Z_{\mathrm{ad}}, \{\mathbf{R}_I\}} E^{\mathrm{tot}}(X_{\mathrm{ad}}, Y_{\mathrm{ad}}, Z_{\mathrm{ad}}, \{\mathbf{R}_I\}) \quad , \tag{10}$$
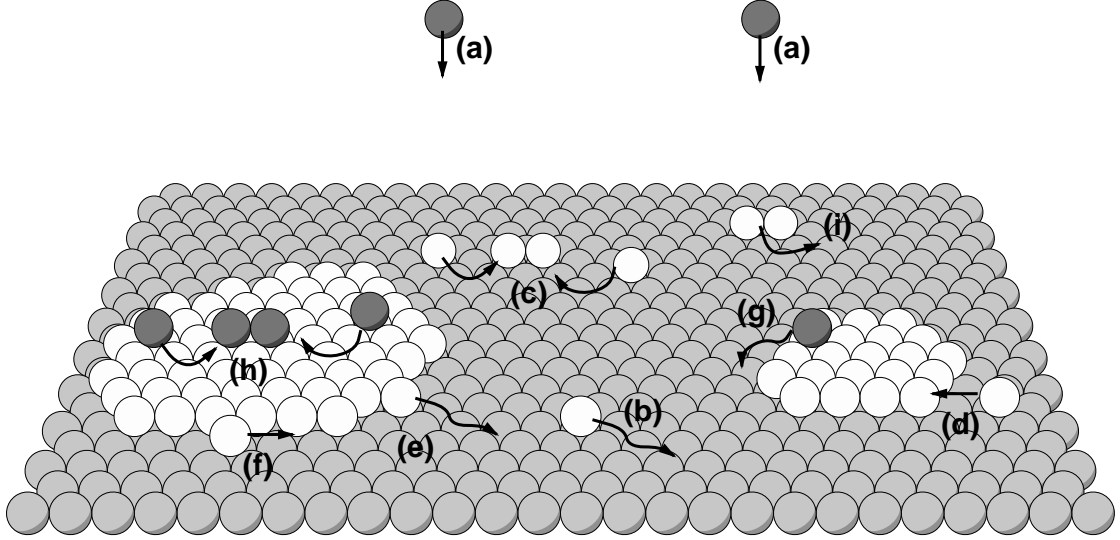
Figure 1: The different atomistic processes for adatoms on a surface. See the text for a discussion.

where $E^{\mathrm{tot}}(X_{\mathrm{ad}}, Y_{\mathrm{ad}}, Z_{\mathrm{ad}}, \{\mathbf{R}_I\})$ is the ground-state energy of the many-electron system (also referred to as the total energy) at the atomic configuration $(X_{\mathrm{ad}}, Y_{\mathrm{ad}}, Z_{\mathrm{ad}}, \{\mathbf{R}_I\})$. According to Eq. (10), the PES is the minimum of the total energy with respect to the z-coordinate of the adatom Z_{ad} and all coordinates of the substrate atoms $\{\mathbf{R}_I\}$. Assuming that vibrational effects can be neglected, the minima of the PES represent stable and metastable sites of the adatom. Note that this PES refers to slow motion of nuclei and assumes that for any atomic configuration the electrons are in their respective ground state. Thus, it is assumed that the dynamics of the electrons and of the nuclei are decoupled (Born-Oppenheimer approximation).

The dynamics of an adatom on such a PES can be described by different approaches. In a molecular dynamics simulation the forces on each atom are computed and the atoms are moved accordingly. Such a simulation is very computer intensive, and we will discuss the advantages and disadvantages in more detail in Section 5. An alternative idea that will be used in this article is that processes such as diffusion are described by rates. Within transition state theory (TST) the rate of a microscopic process j usually has the form [25, 26, 27]

$$\Gamma^{(j)} = \frac{k_{\mathrm{B}}T}{h} \exp(-\Delta F^{(j)}/k_{\mathrm{B}}T) \quad , \tag{11}$$

where $\Delta F^{(j)}$ is the difference in the Helmholtz free energy between the maximum (saddle point) and the minimum (equilibrium site) of the potential curve along the reaction path of the process j. T is the temperature, k_{B} the Boltzmann constant, and h the Planck constant. The free energy of activation $\Delta F^{(j)}$ needed by the system to

move from the initial position to the saddle point is given by

$$\Delta F^{(j)} = E_{\mathrm{d}}^{(j)} - T\Delta S_{\mathrm{vib}}^{(j)} \quad . \tag{12}$$

Here $E_{\mathrm{d}}^{(j)}$ is the sum of the differences in the static total and vibrational energy of the system with the particle at the minimum and at the saddle point, and $\Delta S_{\mathrm{vib}}^{(j)}$ is the analogous difference in the vibrational entropy. The rate of the process j can be cast as follows:

$$\Gamma^{(j)} = \Gamma_0^{(j)} \exp(-E_{\mathrm{d}}^{(j)}/k_{\mathrm{B}}T) \quad , \tag{13}$$

where $\Gamma_0^{(j)} = (k_{\mathrm{B}}T/h)\exp(\Delta S_{\mathrm{vib}}^{(j)}/k_{\mathrm{B}})$ is the effective attempt frequency. In the case of isotropic motion of an adatom on the surface it follows from Eq. (13) that the diffusion constant is $D = D_0 \exp(-E_{\mathrm{d}}^{(j)}/k_{\mathrm{B}}T)$ [28]. The prefactor $D_0 = 1/(2\alpha)\Gamma_0^{(j)}l^2$, where l is the jump length and α the dimensionality of the motion ($\alpha = 2$ for the surface).

The two basic quantities in Eq. (13) are the attempt frequency $\Gamma_0^{(j)}$ and the activation energy $E_{\mathrm{d}}^{(j)}$. TST [26, 27] allows an evaluation of $\Gamma_0^{(j)}$ within the harmonic approximation:

$$\Gamma_0^{(j)} = \frac{\prod_{i=1}^{3N} \nu_i}{\prod_{i=1}^{3N-1} \nu_i^*} \quad , \tag{14}$$

where ν_i and ν_i^* are the normal mode frequencies of the system with the adatom at the equilibrium site and at the saddle point, respectively, and $3N$ is the number of degrees of freedom. The denominator in Eq. (14) contains the product of only $3N - 1$ normal frequencies, because for the adatom at the saddle point one of the modes describes the motion of the particle toward the final site and has an imaginary frequency. TST is only valid when $E_{\mathrm{d}}^{(j)}$ is larger than $k_{\mathrm{B}}T$.

The attempt frequency $\Gamma_0^{(j)}$ shows a much weaker temperature dependence than the exponential and for typical growth temperatures it is of the order $10^{12} - 10^{13} s^{-1}$. When the barriers for two diffusion events are different a *compensation effect* may occur, i.e., $\Gamma_0^{(j)}$ is larger for processes with a higher energy barrier. Indeed, a higher energy barrier usually implies a larger curvature of the potential well around the equilibrium site of the adatom. The corresponding vibrational frequencies of the adatom in such a potential are larger as well, which implies [see Eq. (14)] that the attempt frequency increases. Boisvert *et al.* [29] found that for metal diffusion the prefactor might decrease by up to one order of magnitude for very low energy barriers.

Now consider all possible paths l that describe process j to get from one stable or metastable adsorption site, $\mathbf{R}_{\mathrm{ad}}^{(j)}$, to an adjacent one, $\mathbf{R}_{\mathrm{ad}}^{(j)\prime}$. The energy difference $E_{\mathrm{d}l}^{(j)}$ between the energy at the saddle point along l and the energy of the initial geometry is the barrier for this particular path. If the vibrational energy is negligible compared to $E_{\mathrm{d}l}^{(j)}$, the diffusion barrier $E_{\mathrm{d}}^{(j)}$ then is the minimum value of all $E_{\mathrm{d}l}^{(j)}$ of the possible paths that connect $\mathbf{R}_{\mathrm{ad}}^{(j)}$ and $\mathbf{R}_{\mathrm{ad}}^{(j)\prime}$, and the lowest energy saddle point is called the *transition state*. Although often only the path with the most favorable energy barrier
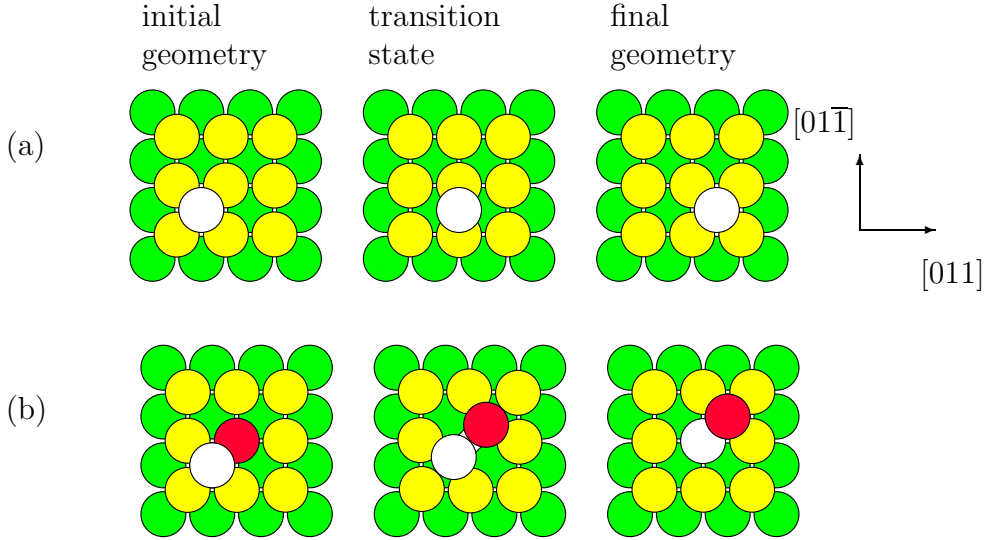
Figure 2: Diffusion via hopping (a) and exchange (b) on a fcc (100) surface.

is important, it may happen that several paths exist with comparable barriers or that the PES consists of more than one sheet (e.g. Ref. [30]). Then the *effective* barrier measured in an experiment or a molecular dynamics (MD) simulation represents a proper average over all possible pathways.

The common view for surface diffusion is that an adatom hops from one lattice site to a neighboring lattice site. This mechanism is called *hopping* and for the (100) surface it is illustrated in Fig. 2(a). Diffusion might also occur with a very different mechanism, the so-called *diffusion by atomic exchange* (or *exchange mechanism*). The adatom can replace a surface atom and the replaced atom then assumes an adsorption site. This was first discussed by Bassett and Webber [31] and Wrigley and Ehrlich [32]. Even for the crystal bulk exchange diffusion has been discussed [33]. This mechanism is actuated by the desire of the system to keep the number of cut bonds low along the diffusion pathway. On fcc (100) surfaces diffusion by atomic exchange was observed experimentally for Pt and Ir [34], and theoretically predicted for Al [35]. The geometry for exchange diffusion at a fcc (100) surface is shown in Fig. 2(b).

If one looks at a diffusion event in an experiment one can often not distinguish the different mechanisms that were operative, so that an experimentally deduced quantity is only an averaged quantity over the different mechanisms. Within TST, one can define an individual rate for each process, for example for surface diffusion via hopping and exchange. In a temperature range where several of these mechanisms are important, one has to take the correct average of them to compare the theoretical values with the experimental ones [30].

3.2 Analysis of Experimental Results

Before discussing results that were obtained for growth parameters from ab initio calculations and comparing them with data obtained from experimental measurements, we would like to briefly outline how experimental data often are analyzed. For simplicity, we will only focus on the surface diffusion constant.

Processes $(a), (b), (c), (d)$, and (e) of Fig. 1 can be described by phenomenological rate equations of the form

$$\frac{dN_1}{dt} = \Phi - 2\kappa_1 N_1^2 - N_1 \sum_{j>1} \kappa_j N_j + 2\gamma_2 N_2 + \sum_{j>2} \gamma_j N_j \tag{15}$$

$$\frac{dN_j}{dt} = N_1(\kappa_{j-1}N_{j-1} - \kappa_j N_j) - \gamma_j N_j + \gamma_{j+1}N_{j+1} \quad . \tag{16}$$

Such a set of equations constitutes the basis of nucleation theory and describes the time evolution of the adatom density, N_1, and the density of islands of size j, N_j, for growth on a flat surface in the submonolayer regime. Adatoms are deposited onto the substrate at a rate $\Phi = F\mathcal{N}$ adatom/s where F is the flux in ML/s and $\mathcal{N}$ the number of atoms pro ML. The second and third term in Eq. (15) account for isolated adatoms being "lost" because two adatoms can meet at a rate κ_1 to form a new nucleus, or adatoms get captured at a rate κ_j by an island of size j. The last two terms in Eq. (15) describe further supply sources of adatoms and are gain terms because dimers may dissociate and adatoms detach from an island of size j at a rate γ_j. Equation (16) reflects the fact that the number of islands of size j increases because islands of size $j-1$ grow and islands of size $j+1$ shrink. The number of islands of size j decreases when islands of size j either shrink or grow. Note that no evaporation into the gas phase is included in Eqs. (15) and (16) (that means that the description in terms of Eqs. (15) and (16) is appropriate only at not too high temperatures).

With the assumption that agglomerates of $i^* + 1$ and more adatoms are stable against break-up ($\gamma_j = 0$ for $j > i^*$) one derives the scaling relation [36]

$$N^{\text{is}} = C_0 \left(\frac{D}{F}\right)^{-i^*/(i^*+2)} \tag{17}$$

where $N^{\text{is}} = \sum_{j>i^*} N_j$ is the island density and D the diffusion coefficient of an adatom on the flat surface. The number i^* is called the size of the critical nucleus. The main steps to derive Eq. (17) are as follows: A steady state for the adatom concentration is assumed, i.e., the left-hand side of Eq. (15) is neglected. This means essentially that the number of adatoms deposited equals the number of atoms captured when all islands on the surface are larger than i^*. Eq. (15) can then be inserted into Eq. (16), and the latter is integrated to obtain Eq. (17). The total island density thus depends on the ratio of the adatom diffusion constant and the deposition flux. When the diffusion constant increases, a deposited adatom can sample a larger area

before the next adatom is deposited. Therefore, the density of island decreases. The same results from a smaller deposition rate, because the time between two successive deposition events increases, and thus again the area sampled by a diffusing adatom is enlarged.

It is widely believed that scaling laws that result from nucleation theory can be applied straightforward, so that measurements of the island density as a function of the growth temperature can yield the barrier for surface diffusion and the prefactor. The results presented in Section 4 of this article show that this bears quite some risks and may lead to incorrect conclusions. Furthermore, it has been shown [37] that relation (17) is problematic for $i^* > 1$ because not always a well defined integer i^* exists. As long as the temperature is small enough (or the deposition rate is large enough), a dimer is essentially stable and $i^* = 1$. When D/F increases, i^* eventually becomes larger than 1, because atoms can break away from any island. In particular, it is plausible that an atom that is singly bonded at the edge of a large cluster is more likely to detach than an atom that is part of a small cluster with all atoms in the cluster being highly coordinated. Thus, the quantity i^* should be interpreted as an effective, averaged quantity, and it is clear that it does not have to take on an integer value. When D/F is small enough $i^* = 1$, and we restrict ourselves to this regime in the present discussion.

In an STM experiment the island density can be measured as a function of the temperature. In a log-log plot of N^{is} as a function as D/F one can obtain E_{d} from the slope of the data, and D_0 from the intercept with the y-axis using Eq. (17) (as long as T is low enough so that $i^* = 1$). This is precisely what is often done in experimental studies. Thus, we would like to stress that a quantity that is often called an *experimental value* is in fact only the result of an *analysis of experimental data*, but not a quantity that is measured directly. An experimentally deduced value for a diffusion barrier and prefactor can not distinguish between different mechanisms such as hopping or exchange, and therefore only represents an effective value that is an average over the different mechanisms.

It is important to note that the analysis is based on certain assumptions. For example, it is possible that not only adatoms, but also clusters diffuse on the surface. In that case, one can still measure the island density, but since cluster diffusion is not included in Eqs. (15) and (16), the scaling law described by Eq. (17) is not applicable anymore, and numbers extracted with it are meaningless. An analysis by Villain *et al.* [38] predicts that the exponent in Eq. (17) can increase in a certain range to 0.5 (for $i^* = 1$) when the diffusion of dimers is allowed. A recent Monte Carlo simulation by Kuipers and Palmer [39] showed that the island density N^{is} decreases significantly when clusters are allowed to diffuse. A decrease of the island density by one order of magnitude leads to an error for the prefactor of $(i^* + 2)/i^*$ orders of magnitude.

The quantity C_0 in Eq. (17) is also not known. It essentially depends on the capture numbers κ_j, and it can be estimated from Monte Carlo simulations to be between 0.1 and 0.5. Using a self consistent approach for the κ_j [40] one gets $C_0 \simeq$

0.25. However, an uncertainty of ~ 5 for C_0 translates also into an uncertainty for the prefactor of two orders of magnitude (for $i^* = 1$). We therefore believe that particularly results obtained for the prefactor from measured island densities using Eq. (17) can be significantly flawed. An improvement of scaling laws that are derived under less restrictive assumptions remains a challenge for the future.

4 STRAIN DEPENDENCE OF SURFACE DIFFUSION

In this Section we will show how the concepts of DFT outlined above can be applied to study surface diffusion. In particular, we will concentrate on the effects of strain on energy barriers and attempt frequencies for metallic systems. We will point out that the analysis of experimental data based on simple scaling laws is more complicated than usually believed.

4.1 Ag on Ag (111) and Pt (111)

Growth of Ag on Pt (111) and Ag on a thin Ag film on Pt (111) has been the focus of recent studies [41, 42]. This system has a lattice mismatch of $4.2\,\%$ and appears to be a well suited system that can provide important information about the effects of strain during growth. Brune *et al.* [41] measured the island densities for Ag on Pt (111), Ag on one monolayer (1 ML) of Ag on Pt (111), and Ag on Ag (111), and employed Eq. (17) to extract the diffusion barriers and prefactors. They obtained $E_{\mathrm{d}}^{\mathrm{Ag\text{-}Pt}} = 157$ meV with $\Gamma_0 = 1 \times 10^{13}$ s^{-1} for Ag on Pt (111), $E_{\mathrm{d}}^{\mathrm{Ag\text{-}Ag/Pt}} = 60$ meV with $\Gamma_0 = 1 \times 10^9$ s^{-1} for Ag on 1 ML Ag on Pt (111), and $E_{\mathrm{d}}^{\mathrm{Ag\text{-}Ag}} = 97$ meV with $\Gamma_0 = 2 \times 10^{11}$ s^{-1} for Ag on Ag (111). In particular for the lowest diffusion barrier the prefactor was found to decrease by 4 orders of magnitude, which the authors of Ref. [41] claim is an unusually high compensation effect.

Not many studies have been devoted to investigate the influence of strain on surface diffusion. The first thorough study we are aware of has been a molecular dynamics simulation for Si on Si (100) that employed a Stillinger-Weber potential [43]. In this study it was found that the barrier for diffusion along the fast channel parallel to the dimer rows is lowered by approximately 10% for 3% compressive as well as for 2% tensile strain, and that atop the dimer rows (in the same direction) it is increased by about 10%. A general trend can not be seen, which might also be due to the fact that the reconstructions for semiconductor systems make the behavior more complicated. For metallic systems there have been a few theoretical studies in the last few years that employed different methods with different degrees of sophistication.

In a recent first principle study [17, 44] the influence of strain on the diffusion constant for Ag on Ag (111) has been discussed. It has been found that in the range of $\pm 5\,\%$ strain the DFT results for the diffusion barrier exhibit a linear dependence
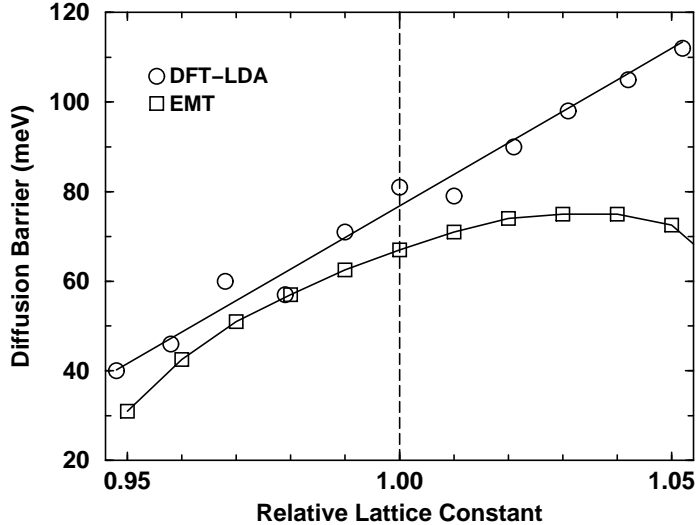
Figure 3: Diffusion barrier (in meV) for Ag on Ag (111) as a function of strain. The circles are DFT-LDA results from Ref. [17] and the squares are EMT results from Ref. [41].

with a slope of 0.7 eV as it is displayed in Fig. 3. The calculated diffusion barrier for the unstrained system, $E_{\mathrm{d}}^{\mathrm{Ag\text{-}Ag}} = 81$ meV, is in good agreement (within the error margins of the experiment and the calculations) with the results obtained from the analysis of the STM measurements of $E_{\mathrm{d}}^{\mathrm{Ag\text{-}Ag}} = 97$ meV. The accordance between experiment and theory extends to the system Ag/Pt (111) and Ag/1ML Ag/Pt (111). These results are summarized in Table 2. In Fig. 3 the DFT-LDA results are compared to those of an EMT study [41]. The EMT results exhibit a linear dependence only for smaller values of strain ($\pm 2\,\%$) and the diffusion barrier starts to decrease for values of misfit larger than $3\,\%$. Indeed, it is plausible that a decrease of the diffusion barrier occurs when the atoms are separated far enough that eventually bonds are broken. However, as the DFT-LDA results show, for Ag/Ag (111) this happens at values for the misfit that are larger than $5\,\%$. Additionally, when comparison with experiment is possible [i.e., Ag on Ag (111), and Ag on a monolayer Ag on Pt (111)] the EMT

Table 2: Diffusion barriers (in meV) for Ag on Pt (111), Ag on one monolayer (ML) Ag on Pt (111), and Ag on Ag (111).

System: Ag on	Experiment [41]	EMT [41]	DFT [17]
Pt (111)	157	81	150
1ML Ag on Pt (111)	60	50	65
Ag (111)	97	67	81

13

Table 3: Prefactor Γ_0 (in THz) and energy barrier E_d (in meV) for strained Ag on Ag (111), and for Ag on one monolayer (ML) Ag on Pt (111). The prefactors are calculated within the harmonic approximation of transition state theory. All results shown were obtained by considering 15 degrees of freedom.

Substrate	Ag (111) $a = 3.92$ Å	Ag (111) $a = 4.05$ Å	Ag (111) $a = 4.22$ Å	1 ML Ag on Pt (111) $a = 3.92$ Å
Γ_0	1.3	0.8	0.3	7.1
E_d	60	81	105	63

results are off by a factor that varies from 1.2 to 2.

The general trend of an increasing energy barrier for hopping diffusion with increasing lattice constant is quite plausible (for exchange diffusion see the next Section). Smaller lattice constants correspond to a reduced corrugation of the surface, and as result the atom is not bonded much stronger at the adsorption sites than at the bridge site. In contrast, when the surface is stretched the corrugation increases and the adsorption energy at the three-fold coordinated hollow sites increases. In an effective medium theory study a linear dependence of the surface diffusion constant as a function of the lattice constant has been found as well for the (111) surfaces of Ni, Pd, Pt, Cu, Ag, and Au [45]. The picture will change when the strain is so large that bonds are broken and then it is expected that the hopping diffusion barrier will start to decrease again at very large tensile strain.

It is worth noting that the diffusion barrier for Ag on top of a pseudomorphic layer of Ag on Pt (111) is substantially lower than it is for Ag on Ag (111). A question that arises is whether this reduced diffusion barrier is a result of the compressive strain or should be ascribed to electronic rearrangements induced by the Pt substrate. The diffusion barrier for Ag on Ag (111) with a lattice constant that is compressed to the value of the lattice constant for Pt is $E_d^{\text{Ag-Ag}} = 60$ meV while that for Ag on Pt (111) (also with the Pt lattice constant of 3.92 Å obtained from DFT) is $E_d^{\text{Ag-Ag/Pt}} = 65$ meV. The agreement of these two values suggests that the reduction of the diffusion barrier for Ag on a layer of Ag on Pt (111) is mainly a strain effect and that the diffusion barrier on top of a layer of Ag is essentially independent of the substrate underneath.

The prefactor for strained Ag on Ag (111) using transition state theory within the harmonic approximation [cf. Eq. (14)] has also been calculated [44]. In this calculation up to 99 degrees of freedom were considered, and it is interesting to note that within a factor of 2 the result agreed with that obtained by taking into account only the degrees of freedom of the moving adatom. It was found that the prefactor changes only very little when the lattice constant (and thus the diffusion barrier, cf. Fig. 3) changes, so that there is no significant compensation effect. The results are summarized in Table 3. All the values calculated are of the order of 1 THz, as

expected, since this is a typical surface phonon frequency. Thus, the calculations do not confirm the claim by the authors of Ref. [41] that there is a very large compensation effect for this system. An additional test has been done to investigate whether the prefactor (in contrast to the diffusion barrier) might be affected by the substrate underneath, but calculations for the prefactor for Ag on 1 monolayer Ag on Pt (111) also gave a prefactor of approximately 1 THz (cf. Table 3).

The reason for the large discrepancy between the theoretical and the experimentally deduced value for the prefactor for the system under compressive strain is not completely understood yet. We believe that the calculations are correct, and that the interpretation of the experimental data may be flawed. Possible reasons for this have been given in the previous Section when we introduced Eq. (17). A low diffusion barrier implies that the PES has a very small corrugation so that it is likely that small clusters diffuse. Also, long range effects (such as reconstructions or strain fields) may become important. The quantity C_0 in Eq. (17) depends on the capture numbers κ_j, but it is not clear how the κ_j behave in a strained system. We thus conclude that one has to be rather careful if one wants to use simple scaling laws to determine microscopic quantities from experimental data.

4.2 Hopping and Exchange Diffusion on (100) Surfaces

As it has been pointed out already in Section 3, diffusion may occur by hopping or atomic exchange on the (100) surface. Fig. 2 shows that the transition state of the exchange mechanism can be described by a dimer, and each atom of this dimer can form three chemical bonds, so that a simple bond counting argument suggests that the exchange mechanism is always the energetically preferred mechanism. It has been calculated by Feibelman [35] that the covalent nature of aluminum which allows the formation of directional bonds at certain geometries lowers the total energy of the system in the transition state for atomic exchange. Thus, the desire of the system to maximize the coordination of all atoms involved is the reason why diffusion proceeds via atomic exchange.

This is certainly a plausible argument for Al (100), but in general chemical bonding is a lot more complicated than counting nearest neighbor bonds and this explanation can not account for atomic exchange as the energetically preferred mechanism for Pt and Ir. Moreover, it is puzzling that for the transition metals Ir and Pt diffusion proceeds via exchange, but according to calculations by Yu and Scheffler [16] for Ag the preferred diffusion mechanism is hopping. The authors of Ref. [16] find that the barrier for hopping is 0.52 eV, while that for exchange is 0.93 eV when the exchange-correlation energy is approximated within the LDA (these numbers change to 0.45 eV and 0.73 eV within the GGA).

In a subsequent paper [46], Yu and Scheffler provided the following explanation for the different behavior of different transition metals. They realized that for $5d$ metals (Ir and Pt, with preferred exchange mechanism) the surface stress is significantly
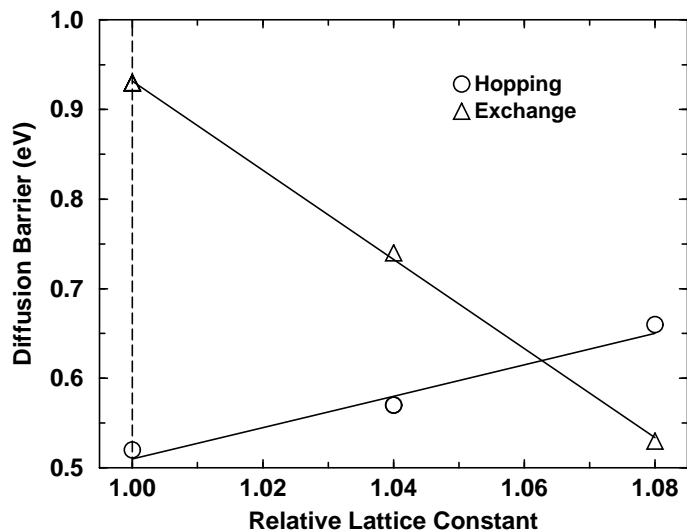
Figure 4: The energy barrier for the hopping and the exchange mechanism for Ag on Ag (100) as a function of the relative lattice constant a/a_0.

higher than it is for $3d$ and $4d$ metals (Ag, where hopping is energetically favored) [47]. This is caused by relativistic effects that play a more important role for the heavier $5d$ metals. Higher tensile surface stress has a tendency to pull the dimer in the transition state for atomic exchange closer toward the surface and the layer underneath to lower the total energy of the system. Thus, under tensile surface stress the barrier for atomic exchange decreases, in contrast to the barrier for hopping, that in analogy to the behavior on the (111) surface is expected to increase under tensile surface stress.

To test this claim, Yu and Scheffler calculated the energy barrier for hopping and exchange as a function of the lattice constant for Ag on Ag (100), and the results are shown in Fig. 4. Indeed, the two curves cross at approximately 6.5% lattice mismatch, and it is predicted that under high tensile surface stress the energetically preferred mechanism is exchange. Yu and Scheffler also claimed that for unreconstructed Au (100) the energetically preferred mechanism should be exchange, with a barrier of 0.65 eV (compared to 0.83 eV for hopping). This again is due to the fact that the dimer in the transition state of the the exchange mechanism is attracted to the surface; it is approximately 37% closer to the surface than the interlayer spacing in the bulk would suggest. This is similar to Al (100), where the dimer is 55% closer to the surface, but in contrast to the (unstrained) Ag (100), where the dimer is only 25% closer to the surface. When Ag (111) is strained by 8% the dimer is 57% closer to the surface.

It seems that there is clear evidence that atomic exchange is stabilized by the correlation of the local coordination of all atoms involved and the strength of the bonds (as for Al), and by the tensile surface stress. Following this argument, the opposite should happen under compressive surface stress: When the surface is compressed, the dimer is "squeezed" away from the surface, and as a result the energy barrier

16

for exchange increases. This is again in contrast to the behavior of the barrier for hopping, that is expected to decrease. Recent results for Al on Al(100) [48] show that indeed the energetically preferred diffusion mechanism changes from exchange to hopping under compressive strain.

Before closing this Section, we would like to point out that based on knowledge for the barrier for surface diffusion it is not appropriate to conclude that one mechanism is the preferred mechanism. The diffusion constant also depends on the prefactor, and there are indications in the literature [49] that the prefactor for diffusion by exchange might be 1 or 2 orders of magnitude larger than the prefactor for hopping. In fact, the consequences of this are discussed in more detail in the example in the next Section. From the results for diffusion of Ag on Ag(111) it can be expected that there is not a significant strain dependence of the prefactor, but more research should be directed toward a better knowledge of the different prefactors for different mechanisms and different surfaces.

5   AB INITIO KINETIC MONTE CARLO SIMULATIONS

The individual microscopic processes can be used to get a deeper understanding of epitaxial growth, provided that their interplay as a function of temperature and deposition rate can be modeled properly. The kinetics during growth is a stochastic process that is well described by a master equation, and the Monte Carlo technique yields a numerical solution of this equation [50, 51]. The master equation governs the dynamic evolution of $P(\sigma, t)$, the probability that the system is in state σ at time t, and it has the following general form:

$$\frac{\partial P(\sigma, t)}{\partial t} = -\sum_{\sigma'} W(\sigma \to \sigma') P(\sigma, t) + \sum_{\sigma} W(\sigma' \to \sigma) P(\sigma', t) \quad . \tag{18}$$

Here $W(\sigma' \to \sigma)$ has the meaning of a transition probability from state σ' to state σ per unit time. On the right-hand side the first sum describes the rate of all processes where the system jumps out of the considered state (and hence decreases its probability), while the second sum describes the rate of all processes where the system jumps into the considered state (and hence increases its probability). The solution of the master equation is achieved computationally by choosing randomly among several possible transitions and accepting or refusing the particular events according to an appropriate probability. In thermal equilibrium the detailed balance condition

$$W(\sigma \to \sigma') P_{\mathrm{eq}}(\sigma) = W(\sigma' \to \sigma) P_{\mathrm{eq}}(\sigma') \tag{19}$$

ensures that the two sums on the right-hand side of Eq. (18) cancel and $P_{\mathrm{eq}}(\sigma)$ is the steady-state distribution of the master equation.

The obvious question concerns the choice of a pertinent transition probability $W(\sigma \rightarrow \sigma')$. The detailed balance criterion, however, only determines the ratio $W(\sigma \rightarrow \sigma')/W(\sigma' \rightarrow \sigma)$. When static properties of the system are sought, the Metropolis algorithm [52] is appropriate. According to this scheme the probability that a new configuration is accepted is proportional to $\exp(-\Delta E/k_\mathrm{B}\mathrm{T})$, where ΔE is the difference between the total energies of the system in the new and old configuration. Such an algorithm searches for the configuration corresponding to the minimum of the total energy. The sequence of generated configurations does not correspond to the real time evolution of the system, and there is no problem of conversion from simulated time t_s to real time t_r. However, for the dynamic behavior (such as growth) of a system the correlation between t_s and t_r is important, and the configuration sequence has to mimic the real one. The appropriate tool for this is KMC. Here the dynamics of the system is obtained from the local microscopic transition rates in terms of Poisson processes.

In contrast to MD, in KMC the place and time of events are no longer deterministically obtained, but are chosen by statistical considerations. The task of the KMC is to build up an artificial chronological sequence of distinct events separated by certain *interevent* times. This chronology is based on the hierarchy dictated by the transition rates and may not correspond to reality. For example, during growth events may occur simultaneously, but KMC introduces an artificial time interval between them. At the other extreme, events may be separated by a very large interval that is not reflected in the KMC *interevent* time. Thus, KMC does not model the "deterministic" microscopic dynamics yielding the exact times of various processes (as MD does). Therefore, in KMC it is possible to avoid the explicit calculation of all unsuccessful attempts, but the chain of events and corresponding interevent times must be constructed from probability distributions weighting appropriately all possible outcomes.

To illustrate the strategy of a KMC simulation (for more details see Ref. [22]) let us consider a system of M particles that are capable of undergoing o total of m transition events (diffusions, deposition, etc.). The m transition events are described by a set of rates $\mathbf{\Gamma} \equiv \{\Gamma^{(1)}, \Gamma^{(2)}, ..., \Gamma^{(m)}\}$ where $\Gamma^{(j)}$ has the form given by Eq. (13). The M particles can be partitioned in classes among the various possible transition events as $\mathbf{M} \equiv \{n^{(1)}, n^{(2)}, ..., n^{(m)}\}$ where $n^{(j)}$ is the number of particles capable of undergoing a transition with a rate $\Gamma^{(j)}$. It should be pointed out that $\sum_j n^{(j)} \geq M$ since a particle may belong to several classes of $\mathbf{M}$ at the same time. Thus, a configuration of the system at a particular time can be labeled by the distribution of $\mathbf{M}$ over $\mathbf{\Gamma}$. A transition is determined by picking randomly among various possible events available at each time step, and the configuration is updated. The choice of the event is dictated by the dynamical hierarchy described by the set of relative transition probabilities $\mathbf{W} \equiv \{W^{(1)}, W^{(2)}, ..., W^{(m)}\}$, each of them defined as:

$$W^{(j)} = \frac{n^{(j)} \Gamma^{(j)}}{R} \quad , \tag{20}$$

18

where $R = \sum_j n^{(j)} \Gamma^{(j)}$ is the total rate. These probabilities are constructed such that detailed balance is achieved at thermal equilibrium. After each Monte Carlo step time should be updated with an increment $\Delta t = -ln(\rho)/R$ where ρ is a random number in the range $(0, 1]$. In this way, a direct and unambiguous relationship between KMC time and real time is established, since the KMC algorithm effectively simulates stochastic processes described by a Poisson distribution.

KMC simulations have been used to study crystal growth of semiconductors (e.g. [53, 54, 55]) and metals (e.g. [56, 57, 58, 59]). However, most of these studies have been based on restrictive approximations. For example, the input parameters have been treated as effective parameters determined rather indirectly by fitting to experimental quantities, like intensity oscillations in helium atom scattering (HAS) measurements or reflection high energy electron diffraction (RHEED), or they were obtained from STM studies of island densities. Thus, the connection between these parameters and the microscopic nature of the processes may be somewhat uncertain. Often the correct surface structure was neglected and the simulation was done on a simple cubic lattice while the system of interest had an fcc or bcc structure. Despite these approximations such studies have provided qualitative and in some cases also quantitative insight into growth phenomena.

It is desirable to carry out KMC simulations with the proper geometry and microscopically well founded parameters. This has been done for example in Refs. [60, 61, 62] where semi-empirical calculations have been employed to evaluate the PES. The most accurate, but also most elaborate approach to obtain the PES employs DFT as described in Sections 2 and 3. It is interesting to note that the result of a KMC study will be the same as that of a MD simulation, provided that the underlying PES is the same. More details on the KMC method are contained in Ref. [22] and references therein.

An example of the possible combination of DFT results and KMC simulations is the study of island shape in functions of substrate temperature for Al on Al(111). This surface, as each (111) surface of an fcc crystal, is characterized by the presence of two types of close-packed steps, labeled as {100} and {111} facets, referring to the plane passing through the atoms of the step and the atom of the substrate (often these steps are labeled A and B). Using the DFT parameters for Al/Al(111) by Stumpf and Scheffler [63, 64] one can carry out KMC simulations under typical growth conditions. The results of the *ab initio* KMC simulations where all relevant processes, including the different mechanisms for a particular event (i.e. hopping or exchange) are included, are shown in Fig. 5. They are obtained after 0.5 s with a deposition rate of 0.8 ML/s. When the growth temperature is 50 K the shape of the islands is highly irregular and indeed fractal. Adatoms which reach a step cannot leave it anymore and they cannot even diffuse along the step. Thus, at this temperature ramification takes place into random directions, and island formation can be understood in terms of the hit and stick model. At $T = 150$ K the island shapes are triangular with their sides being {100}-faceted steps, but increasing the temperature to $T = 200$ K
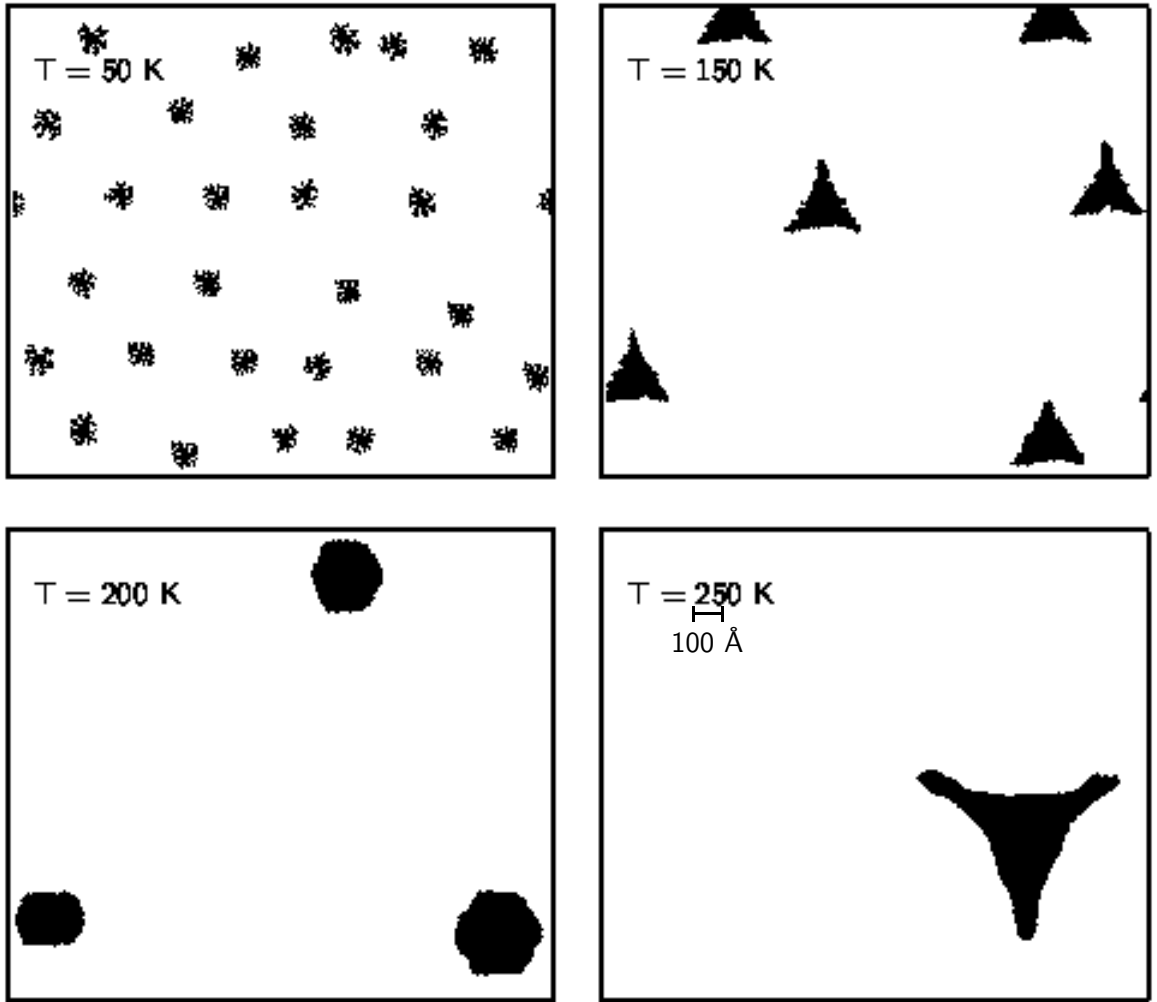
19

Figure 5: A surface area of (1718×1488) Å^2 (half of the simulation area) at four different substrate temperatures. The deposition rate was 0.08 ML/s and the coverage in each picture is $\Theta = 0.04$ ML.

a transition from triangular to hexagonal shape occurs. For $T = 250$ K the islands become triangular again, but they are rotated by π and are mainly bounded by {111}-faceted steps.

The transition can be understood in terms of different diffusivities along the step edges of the islands: The lower the migration probability along a given step edge, the higher is the step roughness and the faster is the speed of advancement of this step edge. As a consequence, this step edge shortens and eventually it may even disappears. Since diffusion along the densely packed steps on the (111) surface (the {100} and {111} facets) is faster than along steps with any other orientation, this criterion explains the presence of islands which are mainly bounded by {100}- or {111}-faceted steps. The same argument can be extended to the diffusion along the

two close-packed steps. By considering the energy barriers (0.32 eV for diffusion along the {100} facet vs. 0.42 eV along the {111}) we would expect only islands with {100} sides, until the temperature regime for the thermal equilibrium is reached. This is the case for $T = 150$ K where the energy barrier dominates the diffusion rate.

DFT calculations [63] have shown that an adatom migrates along the {100} facet by hopping, while along the {111} the diffusion occurs via the exchange mechanism. Since the attempt frequency for exchange is expected to be higher than the one for hopping (in this simulation it is assumed to be two orders of magnitude larger), the higher $\Gamma_0^{\{111\}}$ leads to faster diffusion along the {111} facet than along the {100} one at $T = 250$ K. The latter steps disappear and only triangles with {111}-faceted sides are present. The roughly hexagonally shaped islands at $T = 200$ K are a consequence of the equal advancement speed for the two steps at that temperature. A similar transition in the island shapes has been observed for $\text{Pt}\,(111)$ [65]. An important point regards the time required by the system to assemble these structures. For example, with $F = 0.8$ ML/s the island at $T = 250$ K assumes a triangular shape for $t \geq 0.1$ s, a time not reachable by MD simulations.

In conclusion, during growth the crystal surfaces may show many structural details such as islands, clusters, steps, all of which are originated on an atomic length scale (microscopically well-founded description is needed) but may lead to cooperative phenomena of mesoscopic dimensions with time scale of the order of seconds (stochastic methods are necessary).

6 ACKNOWLEDGMENTS

References

[1] P. Hohenberg and W. Kohn, Phys. Rev. **136**, B864 (1964).

[2] M. Levy, Proc. Natl. Acad. Sci. (USA) **76**, 6062 (1979).

[3] We limit our discussion in this paper to non-magnetic systems. However, it is straightforward to generalize DFT and to write the total-energy functional in terms of the electron density *and* the magnetization density (see for example R.M. Dreizler and E.K.U. Gross, *Density Functional Theory* (Springer Verlag, Berlin, Heidelberg, New York, 1990)).

[4] All equations are noted in Hartree atomic units, i.e., the unit of length is 1 bohr = 0.5292 Å, the unit of energy is 1 hartree = 27.2116 eV, and $\hbar = m = e = 1$.

[5] W. Kohn and L.J. Sham, Phys. Rev. **140**, A1133 (1965).

[6] J.P. Perdew and Y. Wang, Phys. Rev. B **45**, 13244 (1992); J.P. Perdew, in *Electronic Structure of Solids '91*, eds. P. Ziesche and H. Eschrig (Akademie Verlag, Berlin, 1991), p. 11; J.P. Perdew, J.A. Chevary, S.H. Vosko, K.A. Jackson, M.R. Pederson, D.J. Singh, and C. Fiolhais, Phys. Rev. B **46**, 6671 (1992).

[7] J.P. Perdew and Y. Wang, Phys. Rev. B **33**, 8800 (1986); J.P. Perdew, Phys. Rev. B **33**, 8822 (1986); *ibid.* **34**, 7406(E) (1986).

[8] Y. Wang and J.P. Perdew, Phys. Rev. B **43**, 8911 (1991); J.P. Perdew, Physica B **172**, 1 (1991); J.P. Perdew, K. Burke, Y. Wang, unpublished.

[9] A.D. Becke, Phys. Rev. A **38**, 3098 (1988); J. Chem. Phys. **98**, 3892 (1993).

[10] C. Lee, W. Yang, and R.G. Parr, Phys. Rev. B **37**, 785 (1988).

[11] W. Kohn, A.D. Becke, R.G. Parr, J. Chem. Phys. **100**, 12974 (1996).

[12] M. Ernzerhof, J.P. Perdew, and K. Burke, in *Topics in Current Chemistry* **180** (Springer Verlag, Berlin, Heidelberg, New York, 1996), p. 1.

[13] L. Mitas and R.M. Martin, Phys. Rev. Lett. **72**, 2438 (1994); J.C. Grossman, L. Mitas, and K. Raghavachari, Phys. Rev. Lett. **75**, 3870 (1995).

[14] C. Fillipi, X. Gonze, and C.J. Umrigar, to be published in *Recent Developments and Applications of Density Functional Theory*, ed. J.M. Seminario (Elsevier, Amsterdam, 1996).

[15] B. Hammer, M. Scheffler, K.W. Jacobsen, and J.K. Norskov, Phys. Rev. Lett. **73**, 1400 (1994); B. Hammer and M. Scheffler, Phys. Rev. Lett. **74**, 3487 (1995).

[16] B.D. Yu and M. Scheffler, Phys. Rev. Lett. **77**, 1095 (1996); Phys. Rev. B **55**, 13916 (1997).

[17] C. Ratsch, A.P. Seitsonen, and M. Scheffler, Phys. Rev. B **55**, 6750 (1997).

[18] M.C. Payne, M.P. Teter, D.C. Allan, T.A. Arias, and D.J. Joannopoulos, Rev. Mod. Phys. **64**, 1045 (1992).

[19] R. Stumpf and M. Scheffler, Comput. Phys. Commun. **79**, 447 (1994), M. Bockstedte, A. Kley, J. Neugebauer, and M. Scheffler, to be published.

[20] D.J. Singh, *Planewaves, Pseudopotentials, and the LAPW Method* (Kluwer Academic Publ., 1994).

[21] H.L. Skriver, *The LMTO Method* (Springer Verlag, Berlin, Heidelberg, New York, 1983).

[22] P. Ruggerone, C. Ratsch, and M. Scheffler, in *The Chemical Physics of Solid Surfaces* vol. 8, eds. D.A. King and D.P. Woodruff (Elsevier Science, Amsterdam, 1997), in press.

[23] D.C. Senft and G. Ehrlich, Phys. Rev. Lett. **74**, 294 (1995).

[24] T.R. Linderoth, S. Horch, E. Lægsgaard, I. Stensgaard, and F. Besenbacher, Phys. Rev. Lett. **78**, 4978 (1997).

[25] S. Glasston, K.J Laidler, and H. Eyring, *The Theory of Rate Processes*, (McGraw-Hill, New York, 1941).

[26] G.H. Vineyard, J. Phys. Chem. Solids **3**, 121 (1957).

[27] G. Wahnström, in *Interaction of Atoms and Molecules with Solid Surfaces*, eds. V. Bortolani, N.H. March, and M.P. Tosi (Plenum Press, New York and London, 1990), p. 529.

[28] R. Gomer, Rep. Prog. Phys. **53**, 917 (1990).

[29] G. Boisvert, L.J. Lewis, and A. Yelon, Phys. Rev. Lett. **75**, 469 (1995).

[30] A. Kley and M. Scheffler, in *The Physics of Semiconductors*, Eds. M. Scheffler and R. Zimmermann (World Scientific, Singapore, 1996), p. 1031.

[31] D.W. Bassett and P.R. Webber, Surf. Sci. **70**, 520 (1978).

[32] J.D. Wrigley and G. Ehrlich, Phys. Rev. Lett. **44**, 661 (1978).

[33] K.C. Pandey, Phys. Rev. Lett. **57**, 2287 (1986).

[34] G.L. Kellog and P.J. Feibelman, Phys. Rev. Lett. **64**, 3143 (1990); C. Chen and T.T. Tsong, Phys. Rev. Lett. **64**, 3147 (1990).

[35] P.J. Feibelman, Phys. Rev. Lett. **65**, 729 (1990).

[36] S. Stoyanov and D. Kashchiev, in: Vol. 7 of *Current Topics in Materials Science*, Ed. E. Kaldis (North-Holland, Amsterdam, 1981), p. 69.

[37] C. Ratsch, A. Zangwill, P.Šmilauer, and D.D. Vvedensky, Phys. Rev. Lett. **72**, 3194 (1994).

[38] J. Villain, A. Pimpenelli, L. Tang, and D.E. Wolf, J. Phys. I France **2**, 2107 (1992).

[39] L. Kuipers and R.E. Palmer, Phys. Rev. B **53**, R7646 (1996).

[40] G.S. Bales and D.C. Chrzan, Phys. Rev. B **50**, 6057 (1994).

[41] H. Brune, K. Bromann, H. Röder, K. Kern, J. Jacobsen, P. Stolze, K.W. Jacobsen, J. Nørskov, Phys. Rev. B **52**, R14380 (1995).

[42] H. Brune and K. Kern, in *Growth and Properties of Ultrathin Layers*, eds. D.A. King and D.P. Woodruff (Elsevier Science, Amsterdam, 1997), in press; and references therein.

[43] C. Roland and G.H. Gilmer, Phys. Rev. B **46**, 13428 (1992).

[44] C. Ratsch and M. Scheffler, unpublished.

[45] J.J. Mortensen, B. Hammer, O.H. Nielsen, K.W. Jacobsen, and J.K. Nørskov, in *Elementary Processes in Excitations and Reactions*, eds. A. Okiji, H. Kasai, and K. Makoshi (Springer, Berlin 1996), p.173.

[46] B.D. Yu and M. Scheffler, unpublished.

[47] V. Fiorentini, M. Methfessel, and M. Scheffler, Phys. Rev. Lett. **71**, 1051 (1993).

[48] C. Ratsch, V. Bostanov, and M. Scheffler, unpublished.

[49] C.L. Liu, J.M. Cohen, J.B. Adams, and A.F. Voter, Surf. Sci. **253**, 334 (1991).

[50] *The Monte Carlo Method in Condensed Matter Physics*, ed. K. Binder (Springer Verlag, Berlin, Heidelberg, New York, 1992), and references therein.

[51] H.C. Kang and W.H. Weinberg, J. Chem. Phys. **90**, 2824 (1989); K.A. Fichthorn and W.H. Weinberg, J. Chem. Phys. **95**, 1090 (1991); H.C. Kang and W.H. Weinberg, Acc. Chem. Res. **25**, 253 (1992).

[52] M. Metropolis, A.W. Rosenbluth, M.N. Rosenbluth, A.N. Teller, and E. Teller, J. Chem. Phys. **21**, 1087 (1953).

[53] A. Madhukar, Surf. Sci. **132**, 344 (1983); A. Madhukar and S.V. Ghaisas, Appl. Phys. Lett. **47**, 247 (1985); S.V. Ghaisas and A. Madhukar, J. Vac. Sci. Technol. B **3**, 540 (1985); S.V. Ghaisas and A. Madhukar, Phys. Rev. Lett. **56**, 1066 (1986).

[54] S. Clarke and D.D. Vvedensky, Phys. Rev. Lett. **58**, 2235 (1987); Phys. Rev. B **36**, 9312 (1987); Phys. Rev. B **37**, 6559 (1988); J. Appl. Phys. **63**, 2272 (1988); S. Clarke, M.R. Wilby, D.D. Vvedensky, T. Kawamura, K. Miki, and H. Tokumoto, Phys. Rev. B **41**, 10198 (1990); T. Shitara, D.D. Vvedensky, M.R. Wilby, J. Zhang, J.H. Neave, and B.A. Joyce, Phys. Rev. B **46**, 6815 (1992); Phys. Rev. B **46**, 6825 (1992).

[55] H. Metiu, Y.-T. Lu, and Z. Zhang, Science **255**, 1088 (1992).

[56] M.C. Bartelt and J.W. Evans, Phys. Rev. Lett. **75**, 4250 (1995);

[57] Z. Zhang, X. Chen, and M. Lagally, Phys. Rev. Lett. **73**, 1829 (1994).

[58] J.G. Amar and F. Family, Phys. Rev. Lett. **74**, 2066 (1995).

[59] S.V. Khare, N.C. Bartelt, and T.L. Einstein, Phys. Rev. Lett. **75**, 2148 (1995).

[60] S. Liu, Z. Zhang, G. Comsa, and H. Metiu, Phys. Rev. Lett. **71**, 2967 (1993).

[61] J. Jacobsen, K.W. Jacobsen, P. Stolze, and J.K. Nørskov, Phys. Rev. Lett. **74**, 2295 (1995); J. Jacobsen, K.W. Jacobsen, and J.K. Nørskov, Surf. Sci. **359**, 37 (1996).

[62] Z.-P. Shi, Z. Zhang, A.K. Swan, and J.F. Wendelken, Phys. Rev. Lett. **76**, 4927 (1996).

[63] R. Stumpf and M. Scheffler, Phys. Rev. Lett. **72**, 254 (1994); *ibid.* **73**, 508 (1995)(E).

[64] R. Stumpf and M. Scheffler, Phys. Rev. B **53**, 4958 (1996).

[65] T. Michely, M. Hohage, M. Bott, and G. Comsa, Phys. Rev. Lett. **70**, 3943 (1993).